

High-temperature resistivity and thermoelectric properties of coupled substituted $\text{Ca}_3\text{Co}_2\text{O}_6$

This content has been downloaded from IOPscience. Please scroll down to see the full text.

2009 Sci. Technol. Adv. Mater. 10 015007

(<http://iopscience.iop.org/1468-6996/10/1/015007>)

View [the table of contents for this issue](#), or go to the [journal homepage](#) for more

Download details:

IP Address: 129.81.226.78

This content was downloaded on 20/01/2015 at 10:54

Please note that [terms and conditions apply](#).

High-temperature resistivity and thermoelectric properties of coupled substituted $\text{Ca}_3\text{Co}_2\text{O}_6$

Meenakshisundaram Senthilkumar¹ and Rajagopalan Vijayaraghavan²

¹ Chemistry Department, SKP Engineering College, Thiruvannamalai 606 611, Tamil Nadu, India

² Materials and Inorganic Chemistry Division, School of Science and Humanities, VIT University, Vellore 632 014, Tamil Nadu, India

E-mail: rvijayaraghavan@vit.ac.in

Received 24 June 2008

Accepted for publication 5 January 2009

Published 4 March 2009

Online at stacks.iop.org/STAM/10/015007

Abstract

Polycrystalline samples of $\text{Ca}_{3-x}\text{Na}_x\text{Co}_{2-x}\text{Mn}_x\text{O}_6$ ($x = 0.0\text{--}0.5$) have been prepared by the sol-gel cum combustion method using sucrose in order to investigate the effects of the coupled substitution of Na and Mn on Ca and Co sites on the transport properties of $\text{Ca}_3\text{Co}_2\text{O}_6$ (Co326). The products were characterized by Fourier transform infrared spectroscopy, powder x-ray diffraction (XRD), thermogravimetry (TGA), differential thermal analysis and scanning electron microscopy. XRD patterns reveal the formation of single-phase products up to $x = 0.5$. Coupled substitution increases the solubility of both Na and Mn on Ca and Co sites, respectively, in contrast to the limited solubility of Na and Mn ($x = 0.2$) when separately substituted. TGA confirms the formation of the $\text{Ca}_3\text{Co}_2\text{O}_6$ phase at temperatures $\sim 720^\circ\text{C}$. The grain size of the parent and substituted products is in the range 150–250 nm. Electrical resistivity and Seebeck coefficient were measured in the temperature range 300–800 K. Resistivity shows semiconducting behavior for all the compositions, particularly in the low-temperature regime. The Seebeck coefficient increases with temperature throughout the measured temperature range for all compositions. The maximum Seebeck coefficient ($200 \mu\text{V K}^{-1}$) is observed for $x = 0.5$ at 825 K, and this composition may be optimal for high-temperature thermoelectric applications.

Keywords: Seebeck coefficient, resistivity, x-ray diffraction, sol-gel

(Some figures in this article are in colour only in the electronic version)

1. Introduction

Thermoelectric devices recently attracted renewed interest in terms of their potential applications in clean energy conversion systems. At present, materials such as $(\text{Bi}, \text{Sb})_2(\text{Te}, \text{Se})_3$ [1–3], filled skutterudites [4–6] and Si–Ge alloys [7, 8] have the highest thermoelectric performance with the dimensionless figure of merit $ZT = S^2T/\rho\kappa > 1$. Here S , ρ , κ and T are thermoelectric power, electrical resistivity, thermal conductivity and temperature, respectively. However, other than Si–Ge, their applications to power generation are very limited at high temperatures because of the material

decomposition. The thermoelectric performance of oxides is considered as low because of their high electrical resistivity resulting from poor carrier mobility. However, the recent discovery of high thermopower coexisting with low electrical resistivity in NaCo_2O_4 and $\text{Ca}_3\text{Co}_4\text{O}_9$ has opened the way to the exploration of oxide thermoelectric materials [9–12]. Because oxides have the merits of long-time stability in air at high temperature, they may be regarded as promising thermoelectric materials [13, 14]. $\text{Ca}_3\text{Co}_2\text{O}_6$ (Co326) is a decomposed phase of $\text{Ca}_3\text{Co}_4\text{O}_9$ (Co349) and is stable up to 1300 K [15]. It has potential as a better thermoelectric material than Co349 at high temperatures owing to its better

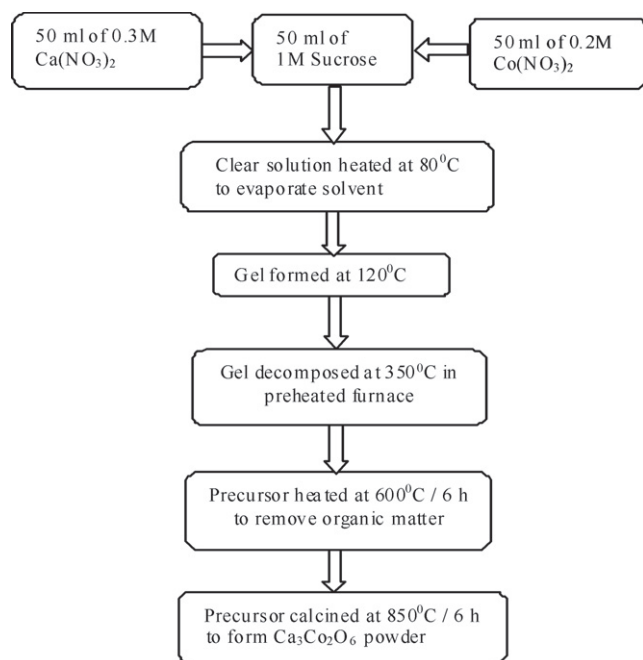


Figure 1. Flowchart of the synthesis of $\text{Ca}_3\text{Co}_2\text{O}_6$.

stability. However, the ZT value of Co326 is only 0.15 at 1073 K [16].

The present study reports the synthesis of pure and substituted Co326 by the sucrose-assisted sol-gel cum combustion method with the objective of obtaining nanocrystalline products. Sucrose has previously been employed as a gelling agent in the sol-gel synthesis of nanocrystalline oxides [17–19]. The effect of the coupled substitution of Na and Mn on the sites of Ca and Co, respectively, in the Co326 phase has been studied to modify the thermoelectric properties of the Co326 phase and also to increase the solubilities of Na and Mn. The coupled substitution of Na and Mn in the Co326 phase has not been reported yet.

2. Experimental work

Polycrystalline samples of $\text{Ca}_{3-x}\text{Na}_x\text{Co}_{2-x}\text{Mn}_x\text{O}_6$ ($x = 0.0-0.5$) were synthesized by the sol-gel cum combustion method using sucrose as a gelling agent. The starting materials were analytical-grade sucrose and nitrates of Ca, Na, Co and Mn. Aqueous solutions of the reactants were prepared according to the molar ratio Ca:Co:sucrose of 0.3:0.2:1 corresponding to the stoichiometry of the $\text{Ca}_3\text{Co}_2\text{O}_6$. The required volumes of the above solutions were then mixed and the resulting solution was heated to a temperature in the range 80–120 °C with constant stirring to obtain the gel. Subsequently, it was decomposed at 350 °C for 0.5 h in a preheated furnace, resulting in a large voluminous fluffy mass of precursor. This precursor was then heated at 600 °C for 6 h to remove carbonaceous material and then calcined in the temperature range 850–900 °C in air for 6–24 h to obtain the Co326 product. The procedure is outlined in figure 1.

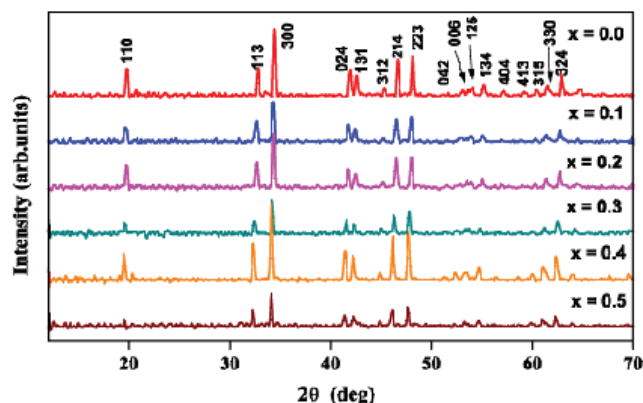


Figure 2. XRD patterns of $\text{Ca}_{3-x}\text{Na}_x\text{Co}_{2-x}\text{Mn}_x\text{O}_6$ ($x = 0.0-0.5$).

X-ray diffraction (XRD) was recorded with a PANalytical ($\text{CuK}\alpha$) X'pert PRO model diffractometer. Lattice parameters were refined by the least squares method. Fourier transform infrared (FTIR) spectra were recorded with a Thermo Nicolet, Avatar 330 spectrometer in the range 400–4000 cm^{-1} using KBr pellets. Thermogravimetry (TG) and differential thermal analysis (DTA) were carried out with a Perkin Elmer instrument in the temperature range 40–1000 °C in air at a heating rate of 10 °C min^{-1} . The morphology of the products was examined using a scanning electron microscope (SEM, Hitachi S-300H). Electrical resistivity ρ of the polycrystalline products was measured by the four-probe dc technique in the temperature range 300–800 K in argon atmosphere. The Seebeck coefficient S was calculated from the plot of thermoelectric voltage against differential temperature in the temperature range 300–800 K in argon atmosphere using Pt–Pt/Rh (R type) thermocouples attached to both sides of the pellets. Pellets of 8 mm diameter and 2 mm thickness for resistivity measurements and 8 mm diameter and 5 mm thickness for thermoelectric measurements were prepared by compacting the calcined powders in WC-lined dies under a pressure of 200 kg cm^{-2} provided by a hydraulic press. The pellets were then sintered at temperature in the range 850–900 °C for 24–36 h. The sodium and oxygen contents were estimated by flame photometry and redox titrations, respectively.

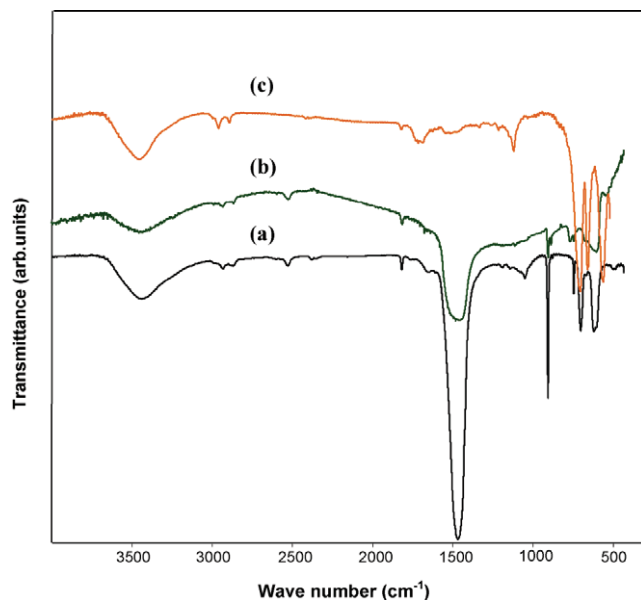
3. Results and discussion

3.1. Sample characterization

3.1.1 Powder XRD. XRD patterns of all the compositions $\text{Ca}_{3-x}\text{Na}_x\text{Co}_{2-x}\text{Mn}_x\text{O}_6$ (figure 2) up to $x = 0.5$ indicate single-phase crystals of the hexagonal structure with lattice parameters $a \cong 0.91$ nm and $c \cong 1.04$ nm. For $x > 0.5$, all samples contain the secondary phase of $\text{Na}_{0.71}\text{Co}_{0.98}\text{O}_2$ [20]. Refined cell parameters are listed in table 1. The cell volume increases with x . Sodium content estimated by flame photometry is consistent with the starting composition. Oxygen stoichiometry estimated by redox titration is 6 ± 0.02 . When Na on the Ca site and Mn on the Co site in the Co326 phase are separately substituted [21], they are soluble only up

Table 1. Refined lattice parameters of $\text{Ca}_{3-x}\text{Na}_x\text{Co}_{2-x}\text{Mn}_x\text{O}_6$ ($x = 0.0-0.5$).

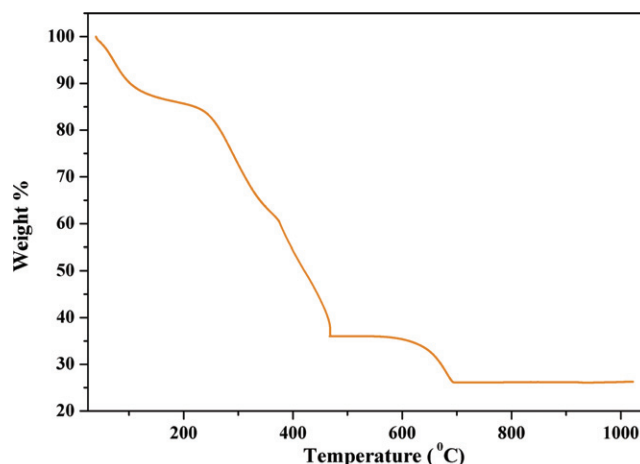
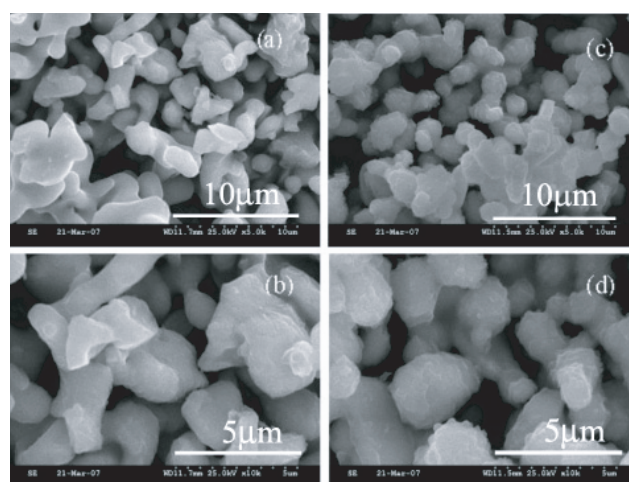
Composition (x)	a (nm)	c (nm)	Volume (nm^3)
0.0	0.904(4)	1.035(4)	0.734
0.1	0.904(6)	1.036(4)	0.735
0.2	0.906(2)	1.037(4)	0.738
0.3	0.908(2)	1.044(2)	0.746
0.4	0.910(2)	1.048(3)	0.752
0.5	0.911(5)	1.046(4)	0.753

**Figure 3.** FTIR spectra of precursor of $\text{Ca}_3\text{Co}_2\text{O}_6$ calcined at (a) 600 °C, (b) 800 °C and (c) 850 °C.

to $x = 0.2$, whereas with coupled substitution, the solubilities of Na and Mn are increased up to $x = 0.5$.

3.1.2 FTIR. FTIR spectra of the precursor of Co326 heated at different temperatures are shown in figure 3. The intense bands at 1441 and 875 cm^{-1} (figures 3(a) and (b)), observed in the precursor calcined at 600 and 800 °C, correspond to carbonates [22]. The intensity of carbonate peaks decreases with increasing calcination temperature. In the precursor heated at $T > 850$ °C, the carbonate peak completely vanishes (figure 3(c)) and new bands appear at 670 and 588 cm^{-1} (figure 3(c)). Those bands are assigned to Ca–O and Co–O stretching vibrations [23]; they indicate that the product is formed completely by calcination of the precursor in the temperature range 850–900 °C.

3.1.3 TG and DTA. Figure 4 shows the TG/DTA results of the precursor calcined at 350 °C. The initial weight loss of about 12% in the TG curve is due to the evaporation of adsorbed water. The intermediate weight loss of about 50% in the temperature range 290–470 °C corresponds to the decomposition of organic compounds that likely leads to the formation of CaCO_3 and Co_3O_4 [23]. Calcium carbonate decomposition takes place in the temperature range

**Figure 4.** TGA of precursor of $\text{Ca}_3\text{Co}_2\text{O}_6$.**Figure 5.** (a) and (b) SEM micrographs of $\text{Ca}_3\text{Co}_2\text{O}_6$ and (c) and (d) of $\text{Ca}_{2.8}\text{Na}_{0.2}\text{Co}_{1.8}\text{Mn}_{0.2}\text{O}_6$ under different magnifications.

600–700 °C with the final weight loss of ~12% indicating that Co326 begins to form at ~720 °C.

3.1.4 SEM. SEM images (figure 5) of $x = 0.0$ and 0.2 samples under different magnifications show that the grains of the parent Co326 are well formed into a polyhedral shape, whereas those of substituted Co326 are nearly spherical. The grain sizes in both samples vary between 150 and 250 nm. The crystallite size obtained from XRD patterns using the Scherrer formula is in the range 40–100 nm.

3.2. Transport measurements

3.2.1 Electrical resistivity. Figure 6 presents electrical resistivity ρ of polycrystalline pure Co326 and substituted Co326 phases as a function of temperature in the range 300–800 K. For all the compositions, a semiconductor-like temperature ($d\rho/dT < 0$) is observed; the substituted phases showing weaker temperature dependences than the parent ($x = 0$) phase. Electrical resistivity decreases with x up to $x = 0.2$, but for $x \geq 0.3$, electrical resistivity increases

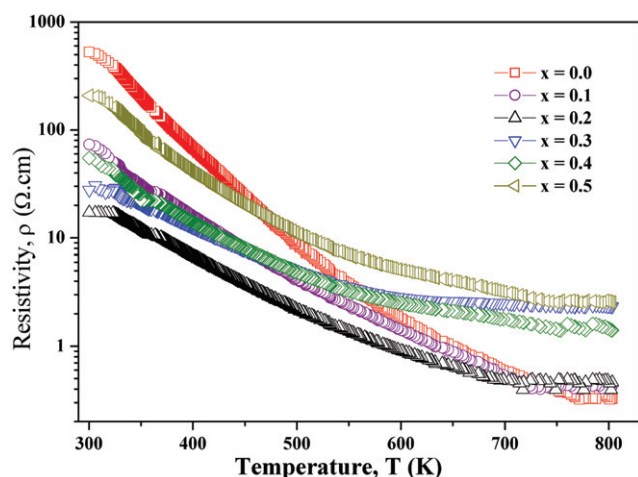


Figure 6. Temperature dependence of resistivity for $\text{Ca}_{3-x}\text{Na}_x\text{Co}_{2-x}\text{Mn}_x\text{O}_6$ ($x = 0.0-0.5$).

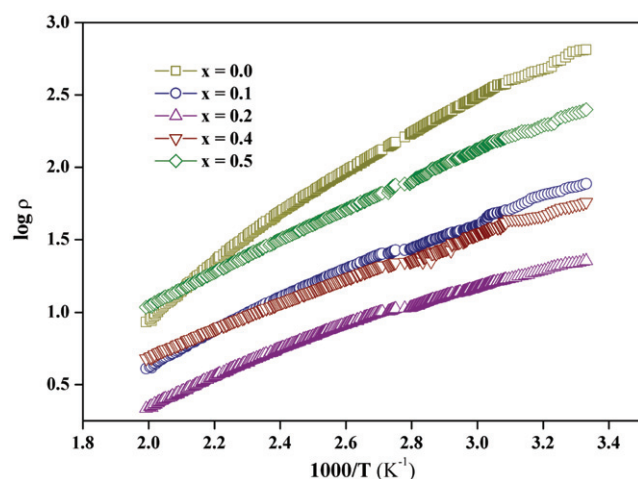


Figure 7. Plot of $\log \rho$ versus $1000/T$ for $\text{Ca}_{3-x}\text{Na}_x\text{Co}_{2-x}\text{Mn}_x\text{O}_6$ ($x = 0.0-0.2$ and $0.4-0.5$) in the temperature range 300–500 K.

with x . This indicates that up to $x = 0.2$, the holes created by the substitution of Na at the Ca site play a dominant role in reducing the resistivity caused by the increase of carrier concentration. However, for $x \geq 0.3$, scattering by Mn and the reduction in carrier concentration may play a more dominant role in increasing the resistivity, as reported for the Co349 phase [24]. This also indicates that these substituted phases are free of the Na_xCoO_2 phase, which is expected to be more conducting [21]. Note however that grain boundary effects, band structure changes upon substitution, oxygen non-stoichiometry and anisotropy of the crystal structure of Co326 also contribute to its transport properties.

Figure 7 presents an Arrhenius plot of $\log \rho$ versus $1/T$ in the temperature range 300–500 K for different x . The parent ($x = 0$) and substituted phases exhibit an activation energy ~ 0.3 eV. The temperature dependence of resistivity is not reversible during heating and cooling cycles. This might cause the deviation from the $1000/T$ activation at high temperatures.

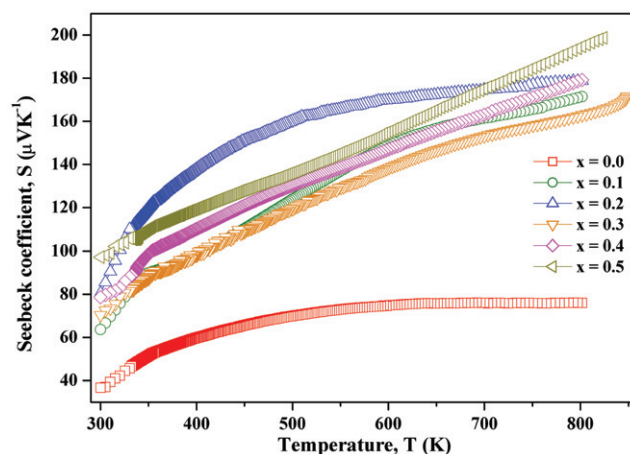


Figure 8. Temperature dependence of Seebeck coefficient S for $\text{Ca}_{3-x}\text{Na}_x\text{Co}_{2-x}\text{Mn}_x\text{O}_6$ ($x = 0.0-0.5$).

3.2.2 Seebeck coefficient. Figure 8 shows the plot of the Seebeck coefficient S as a function of temperature. In all the compositions, S increases with temperature in the range 300–800 K; S is positive indicating p-type transport. The parent phase of Co326 in this study shows an increase of the Seebeck coefficient from 40 to $70 \mu\text{V K}^{-1}$ in the temperature range 300–800 K, in contrast to the previous studies: Takahashi *et al* [25] observed that in single-crystal $\text{Ca}_3\text{Co}_2\text{O}_6$, the Seebeck coefficient increases from $165 \mu\text{V K}^{-1}$ at 300 K to a maximum of $300 \mu\text{V K}^{-1}$ at 440 K and then decreases gradually to $100 \mu\text{V K}^{-1}$ at 1000 K. Iwasaki *et al* [26] observed that in polycrystalline $\text{Ca}_3\text{Co}_2\text{O}_6$, the Seebeck coefficient decreases from 600 to $140 \mu\text{V K}^{-1}$ in the temperature range 300–1200 K. These variations may be attributed to the oxygen non-stoichiometry effects, which have not yet been investigated in the Co326 phase. Note that in LaCoO_3 , the magnitude of the Seebeck coefficient and its temperature dependence are affected by oxygen defects [27].

The substituted phases of $\text{Ca}_{3-x}\text{Na}_x\text{Co}_{2-x}\text{Mn}_x\text{O}_6$ ($x = 0.0-0.5$) show, in general, an increase of S with temperature in the range 300–800 K (figure 8). In these substituted Co326 phases, S increases significantly from 70 to $200 \mu\text{V K}^{-1}$ in the measured temperature range; the $x = 0.5$ samples show the maximum S value of $200 \mu\text{V K}^{-1}$. However, when Na and Mn are substituted separately, S decreases with temperature [21]. An increase of the Seebeck coefficient from 50 to $200 \mu\text{V K}^{-1}$ in the temperature range 300–800 K is observed when Ca is partially substituted by La, Bi, Y and Cr in Co sites in the Co326 phase [26], similar to the substituted phases of $\text{Ca}_{3-x}\text{Na}_x\text{Co}_{2-x}\text{Mn}_x\text{O}_6$. The maximum S value ($200 \mu\text{V K}^{-1}$) observed at 825 K for the composition with $x = 0.5$ in $\text{Ca}_{3-x}\text{Na}_x\text{Co}_{2-x}\text{Mn}_x\text{O}_6$ is marginally higher than that of the mono substituted (Na on Ca and Mn on Co sites separately) Co326 phase at 825 K [21]. Hence, this composition ($x = 0.5$) may be optimal for high-temperature thermoelectric applications.

3.3. Power factor

The temperature variation of the thermoelectric power factor (calculated from the measured ρ and S values) is

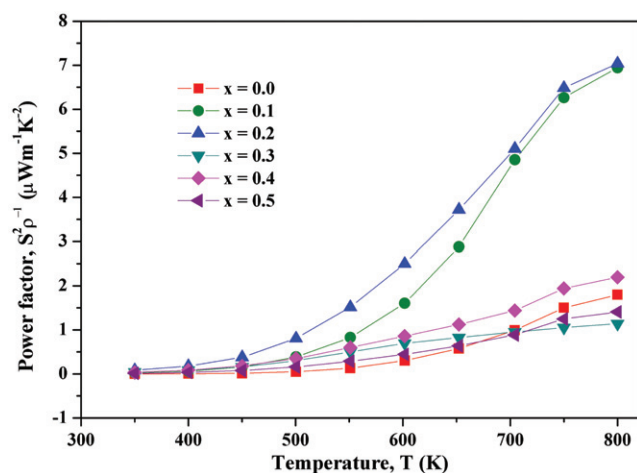


Figure 9. Temperature dependence of power factor for $\text{Ca}_{3-x}\text{Na}_x\text{Co}_{2-x}\text{Mn}_x\text{O}_6$ ($x = 0.0-0.5$).

shown in figure 9. The power factor increases for all compositions with increasing temperature. Its maximum value is $7.03 \mu\text{W m}^{-1}\text{K}^{-2}$ for $x = 0.2$ at 800 K, and this value is comparable to those of the reported substituted phases of $\text{Ca}_3\text{Co}_2\text{O}_6$ at 800 K [21, 26]. For this composition, the figure of merit ZT is 0.0013. In $\text{Ca}_{3-x}\text{Na}_x\text{Co}_{2-x}\text{Mn}_x\text{O}_6$, $x = 0.2$ may be the optimal composition.

4. Conclusion

$\text{Ca}_3\text{Co}_2\text{O}_6$ was synthesized by the sucrose-assisted sol-gel cum combustion method. Coupled substitution of Na and Mn on Ca and Co sites improved the transport properties of $\text{Ca}_{3-x}\text{Na}_x\text{Co}_{2-x}\text{Mn}_x\text{O}_6$ phases. The solubilities of Na and Mn were increased up to $x = 0.5$ by coupled substitution. Electrical resistivity was significantly reduced by the simultaneous substitution of Na and Mn at $x = 0.2$. The Seebeck coefficient increased with increasing x . The maximum value $S = 200 \mu\text{V K}^{-1}$ was observed for the composition with $x = 0.5$. The power factor reached $7.03 \mu\text{W m}^{-1}\text{K}^{-2}$ for $x = 0.2$ at 800 K. To understand the variation of the Seebeck coefficient with temperature, it is necessary to measure the carrier density and band gap. A systematic study of the effects of oxygen nonstoichiometry on the transport properties of these Co326 phases is under way.

Acknowledgments

RV wishes to dedicate this paper in honor of Professor C N R Rao FRS on his 75th birthday. We thank the VIT management and DRDO, Government of India, for funding,

Professor U V Varadaraju, IIT Madras, for help in transport measurements and VIT-TBI for FTIR measurements.

References

- [1] Perrin D, Chitroub M, Scherrer S and Scherrer H 2000 *J. Phys. Chem. Solids* **61** 1687
- [2] Yamashita O, Tomiyoshi S and Makita K 2003 *J. Appl. Phys.* **93** 368
- [3] Cao Y Q, Zhao X B, Zhu T J, Zhang X B and Tu J P 2008 *Appl. Phys. Lett.* **92** 143106
- [4] Sales B C, Mandrus D and Williams R K 1996 *Science* **272** 1325
- [5] Nolas G S, Kaeser M, Littleton R T and Tritt T M 2000 *Appl. Phys. Lett.* **77** 1855
- [6] Chen L D, Kawahara T, Tang X F, Goto T and Hirai T 2001 *J. Appl. Phys.* **90** 1864
- [7] Heller M W, Nasby R D and Johnson Jr R T 1976 *J. Appl. Phys.* **47** 4113
- [8] Mahan G D 1998 *Solid State Physics* vol 51 ed H Ehrenreich and F Spaepen (New York: Academic) p 81
- [9] Terasaki I, Sasago Y and Uchinokura K 1997 *Phys. Rev. B* **56** R 12685
- [10] Fujita K, Mochida T and Nakamura K 2001 *Japan J. Appl. Phys.* **40** 4644
- [11] Li S, Funahashi R, Matsubara I, Ueno K and Yamada H 1999 *J. Mater. Chem.* **9** 1659
- [12] Funahashi R, Matsubara I, Ikuta H, Takeuchi T, Mizutani U and Sodeoka S 2000 *Japan J. Appl. Phys.* **39** L1127
- [13] Funahashi R, Matsubara I and Sodeoka S 2000 *Appl. Phys. Lett.* **76** 2385
- [14] Takahata K, Iguchi Y, Tanaka D and Itoh T 2000 *Phys. Rev. B* **61** 12551
- [15] Fjellvåg H, Gulbrandsen E, Aasland S, Olsen A and Hauback B C 1996 *J. Solid State Chem.* **124** 190
- [16] Mikami M, Funahashi R, Yoshimura M, Mori Y and Sasaki S 2003 *J. Appl. Phys.* **94** 6579
- [17] Wu Y, Bandyopadhyay A and Bose S 2004 *Mater. Sci. Eng.* **380** 349
- [18] Lazarraga M G, Pascual L, Gadjov H, Kovacheva D, Petrov K, Amarilla J M, Rojas R M, Martin-Luengo M A and Rojo J M 2004 *J. Mater. Chem.* **14** 1640
- [19] Prabhakaran K, Jorly J, Gokhale N M, Sharma S C and Ramji L 2005 *Ceram. Int.* **31** 327
- [20] Fousassier C, Matejeka G, Jean-Mauriu R and Hagenmuller P 1973 *J. Solid State Chem.* **6** 5323
- [21] Mikami M and Funahashi R 2005 *J. Solid State Chem.* **178** 1670
- [22] Jiu J, Ge Y, Li X and Nie L 2002 *Mater. Lett.* **54** 260
- [23] Zhang Y F, Zhang J X, Lu Q M and Zhang Q Y 2006 *Mater. Lett.* **60** 2443
- [24] Li D, Qin X Y, Gu Y J and Zhang 2005 *Solid State Commun.* **134** 235
- [25] Takahashi J, Yamane H and Shimada M 2004 *Japan J. Appl. Phys.* **43** L331
- [26] Iwasaki K, Yamane H, Kubota S, Takahashi J and Shimada M 2003 *J. Alloys Compd.* **35** 210
- [27] Iwasaki K, Ito T, Nagasaki T, Arita Y, Yoshino M and Matsui T 2008 *J. Solid State Chem.* **181** 3145